Dynamics of a suspended nanowire driven by an ac Josephson current in an inhomogeneous magnetic field

Milton E. Peña-Aza

Department of Physics, University of Gothenburg, SE-412 96 Göteborg, Sweden

We consider a voltage-biased nanoelectromechanical Josephson junction, where a suspended nanowire forms a superconducting weak link, in an inhomogeneous magnetic field. We show that a nonlinear coupling between the Josephson current and the magnetic field generates a Laplace force that induces a whirling motion of the nanowire. By performing an analytical and a numerical analysis, we demonstrate that at resonance, the amplitude-phase dynamics of the whirling movement presents different regimes depending on the degree of inhomogeneity of the magnetic field: time independent, periodic, and chaotic. Transitions between these regimes and attractor merging crisis are also discussed.

PACS number(s): 05.45.−a, 74.45.+c, 85.85.+j, 85.25.Cp

I. INTRODUCTION

Over the past 15 years, nanoelectromechanical systems (NEMS) have been widely used for the exploration of the quantum world and for the development of new technological applications [1–7]. Because of their size, high frequency operation, small mass, and high performance, NEMS are currently considered promising candidates for achieving the quantum limit of mechanical motion. It is expected that the quest for the quantum regime in such devices will elucidate questions of fundamental nature in physics, for instance, the quantum-mechanical description of macroscopic objects [8–13]. Similarly, physical systems involving NEMS resonators are excellent tools for theoretical and experimental studies of nonlinear dynamical systems [14,15]. Indeed, examples of complex dynamical phenomena in NEMS are numerous and include chaotic behavior [16–19], bifurcation-topology amplification [20], nonlinear switching dynamics [21], and nonlinear frequency pulling [22], to name but a few.

By making use of the potential offered by NEMS resonators, Sonne *et al.* [23] studied the nonlinear dynamics of a suspended carbon nanotube coupled to two voltage-biased superconducting electrodes. In presenting their work, Sonne and collaborators assumed that the nanoelectromechanical junction was subjected to a *homogeneous* magnetic field perpendicular to the axes of the nanowire. For such a system, the authors demonstrated the possibility to pump energy from the electronic subsystem into the mechanical vibrations; they also demonstrated that the system had more than one regime of finite-amplitude stationary nonlinear oscillations. In particular, a region of bistability was found and the authors showed that it should be detected in the corresponding dc Josephson current (see discussion in Ref. [23]).

In this article, we consider the same voltage-biased nanoelectromechanical system studied by Sonne and co-workers [23], but now extend the analysis to a case in which the NEMS resonator is subjected to a *nonuniform* magnetic field. As will be discussed in the following, inhomogeneity of the field causes the conducting nanoresonator to execute a whirling movement resembling a jump-rope-like motion. The purpose of this paper is to analyze the time evolution of the amplitude and relative phase of the nanotube whirling motion. We will demonstrate that the coupled amplitude-phase dynamics exhibits different stationary regimes depending on the degree of the magnetic field inhomogeneity: time independent, periodic, and chaotic.

The scope of this article is parallel to research conducted by Conley *et al.* [24] and Chen *et al.* [25], who previously investigated nonlinear and nonplanar dynamics of suspended nanowires excited by an electrostatic force. Here, however, we consider another type of driving mechanism: the Laplace force, i.e., the force that acts on a current-carrying wire in a magnetic field. This excitation mechanism to accomplish whirling motion of suspended nanoresonators has not been considered before.

The article is organized in the following manner. In Sec. II, we examine the coupling between the mechanical and electronic subsystems and introduce the model Hamiltonian for the considered system. At the end of the section, we derive the equations of motion governing the dynamics of the nanoresonator driven by an ac Josephson current. In Sec. III, we obtain the differential equations for the time evolution of the amplitudes of the nanotube vibration and discuss their dynamics through the analysis of the numerically computed results. Finally, in Sec. IV, we provide the summary and concluding remarks of this work.

II. MODEL HAMILTONIAN SYSTEM

The diagram in Fig. 1 is a schematic illustration of a superconducting hybrid nanostructure, a superconducting-normal-superconducting (S-N-S) nanoelectromechanical Josephson junction driven by a dc voltage bias V. The junction consists of a metallic carbon nanotube of length L suspended between two voltage-biased superconducting leads. In such a geometry, the nanotube is simultaneously serving as a mechanical resonator and as a weak link between the superconducting electrodes. The phase difference between the weakly coupled leads will be denoted by ϕ and, in accordance to the second Josephson relation, its time evolution is $\phi(t) = \omega_J t$, with $\omega_J = 2\,eV/\hbar$ the Josephson frequency. In the layout of the system, the NEMS junction is under the influence of an external inhomogeneous magnetic field **H**, generated by a magnetic force microscope (MFM) cantilever tip in the form of a wedge, parallel to the axis of the nanotube at a distance d. Considering a magnetic field

(a)

(b)
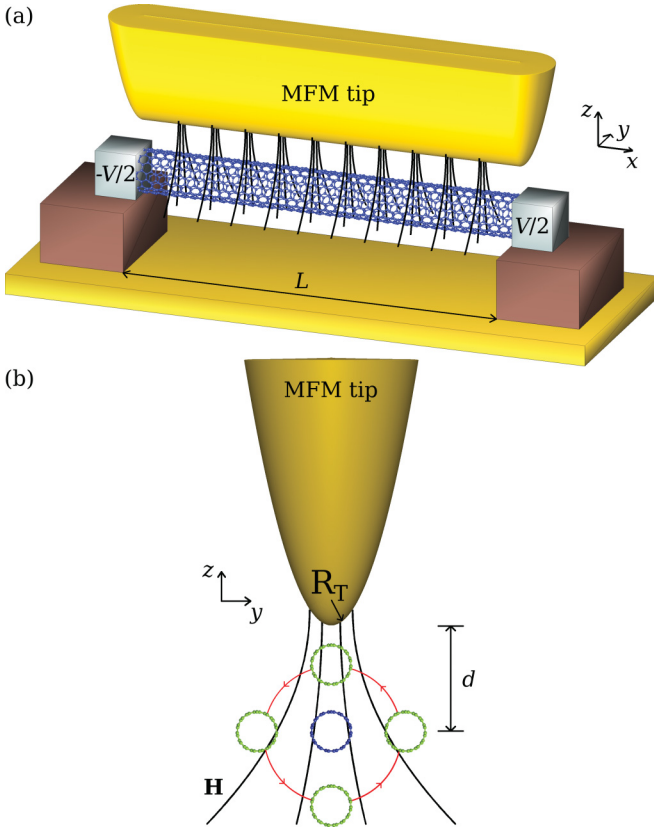
FIG. 1. (Color online) (a) Schematic diagram of the voltage-biased S-N-S nanoelectromechanical Josephson junction considered in the article. A doubly clamped metallic carbon nanotube suspended over a trench of length L forms a weak link between two voltage-biased superconducting electrodes. The junction is influenced by an inhomogeneous magnetic field **H**, generated by a wedge-shaped MFM cantilever tip at a distance d from the nanotube at rest (blue, center, circle). (b) Nanotube displacement (green, outer, circles) in the z-y plane induced by a Laplace force. R_T is the curvature radius of the magnetic tip.

of the form $\mathbf{H} = (0, H_y, H_z)$, a first order Taylor expansion of the magnetic field yields $\mathbf{H} = [0, y\partial_y H_y(x,0,0), H_z(x,0,0) + z\partial_z H_z(x,0,0)]$, where $H_z(x,0,0)$ and $\partial_i H_i(x,0,0)$ represent the magnitudes of, respectively, the magnetic field z component and the magnetic field gradients, both evaluated at the axis of the nanotube. A straightforward calculation from the Maxwell equation $\nabla \cdot \mathbf{H} = 0$ indicates that $\partial_y H_y(x,0,0) = -\partial_z H_z(x,0,0) \equiv -H_z'$. Setting $H_z(x,0,0) \equiv H_z$, the magnetic field reads as

$$\mathbf{H} = (0, -H_z'y, H_z + H_z'z). \tag{1}$$

This field is also obtained from the equation $\mathbf{H} = \nabla \times \mathbf{A}$, with the vector potential $\mathbf{A}$ is given by

$$\mathbf{A} = -([H_z + H_z'z]y, 0, 0). \tag{2}$$

In this scenario, the coupling between the Josephson current and the inhomogeneous magnetic field gives rise to a nonplanar whirling displacement of the nanotube due to the Laplace force. As a consequence of the motion in the magnetic field, an electromotive force is induced along the nanomechanical weak link and its magnitude depends on the rate of change of

the nanowire profile in the z-y plane, i.e., the rate of change of the magnetic flux through the circuit. In this description, now, the superconducting phase difference is not only a function of the bias voltage, but also of the nanowire deflection in the z-y plane. We decompose the nanotube motion in this plane into two independent deflections $y(x,t) = u_0(x)a(t)$ and $z(x,t) = u_0(x)b(t)$, where $u_0(x)$ is the normalized and dimensionless profile of the fundamental mode in both directions. Then, the expression for the superconducting phase difference has the form

$$\varphi(t) = \frac{\phi(t)}{2} + \frac{eL}{4\hbar}[h_z + h_z'b(t)]a(t). \tag{3}$$

The parameters $h_z = \alpha H_z$ and $h_z' = \beta H_z'$ are the renormalized magnetic field and magnetic field gradient in the z direction calculated at the axis of the tube, respectively, with $\alpha, \beta \sim 1$ correctional factors originating from geometrical considerations. The nanotube mechanics is thus described through the projection amplitudes $a(t)$ and $b(t)$ and for the conjugate variables $\{a(t), p_a(t)\}$ and $\{b(t), p_b(t)\}$ $[p_j(t)$ denoting the generalized momenta] one can formulate the following Hamiltonian function:

$$H(p_a, p_b, a, b, t) = \frac{1}{2m}(p_a^2 + p_b^2) + \frac{m\omega^2}{2}(a^2 + b^2)$$
$$- 2D\Delta_0 \cos[\varphi(a,b,t)], \tag{4}$$

where m and ω are the mass and the mechanical eigenfrequency of the nanoresonator, respectively. The last term in Eq. (4) corresponds to the Josephson energy $E_J[\varphi(a,b,t)]$, with D the transmission coefficient of the junction and Δ_0 the superconducting order parameter. The equations of motion for $a(t)$ and $b(t)$ are then obtained from the Hamilton equations. Written in terms of the dimensionless deflection coordinates $Y(t) = [eLh_z/4\hbar]a(t)$ and $Z(t) = [eLh_z/4\hbar]b(t)$, the resulting set of differential equations for the nanotube amplitudes is

$$\ddot{Y}(\tau) + \tilde{\gamma}\dot{Y}(\tau) + Y(\tau)$$
$$= -\varepsilon[1 + \varkappa Z(\tau)]\sin(\tilde{V}\tau + [1 + \varkappa Z(\tau)]Y(\tau)), \tag{5a}$$
$$\ddot{Z}(\tau) + \tilde{\gamma}\dot{Z}(\tau) + Z(\tau)$$
$$= -\varepsilon\varkappa Y(\tau)\sin(\tilde{V}\tau + [1 + \varkappa Z(\tau)]Y(\tau)). \tag{5b}$$

Here, we have added a dimensionless phenomenological damping coefficient $\tilde{\gamma} = [\gamma/m\omega]$. In these equations, $\varepsilon = [2eL^2h_z^2j_c/m\hbar\omega^2]$ with $j_c = [D\Delta_0e/2\hbar]$, the critical current through the junction. We also set the time scale to $\tau = \omega t$ and, consequently, $\tilde{V} = [eV/\hbar\omega]$. The parameter

$$\varkappa = \frac{4\hbar}{eLh_z R_T}, \tag{6}$$

where $R_T = [h_z/h_z']$ denotes the curvature radius of the magnetic cantilever tip, characterizes the degree of inhomogeneity of the magnetic field and will be referred to as the *control parameter*. It turns out that $\varkappa$ determines the dynamical behavior of the system. One can then realize the significance of $\varkappa$ by considering fixed system parameters (L, h_z) and by letting R_T vary. In the limit $R_T \to \infty$, the control parameter vanishes and the equations of motion given by Eqs. (5) reduce to the case discussed by Sonne *et al.* [23] where the magnetic
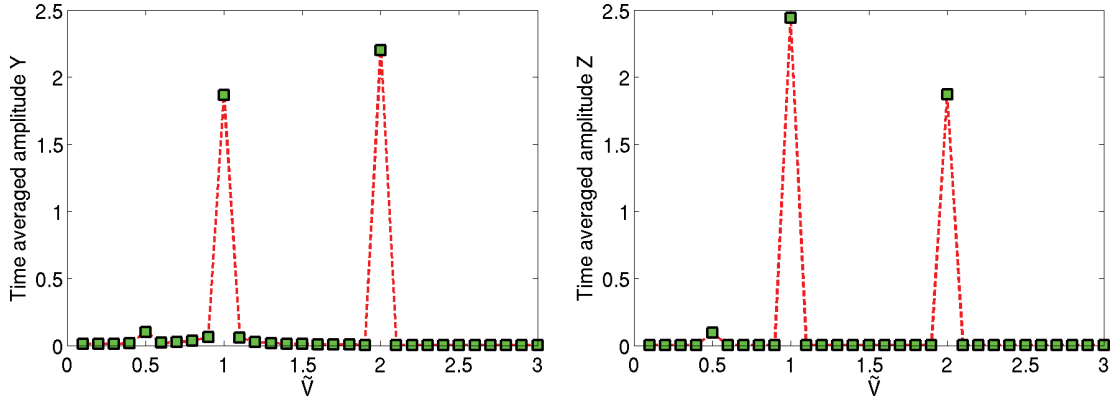
FIG. 2. (Color online) Numerical simulations of Eqs. (5a) and (5b) for the time averaged coordinates Y and Z as a function of the driving voltage $\tilde{V}$. The system presents a series of resonance peaks at integer values of the driving voltage and the amplitude of the nanotube is not damped when the Josephson frequency matches the mechanical frequency. Further analysis is performed at parametric resonance $\tilde{V} = 2$. The plots are calculated for $\tilde{\gamma} = 0.001$, $\varepsilon = 0.012$, $\varkappa = 1$ ($L = 1 \ \mu$m, $h_z = 40$ mT, $R_T = 66$ nm).

field is uniform and, therefore, the amplitude of the driving force acting in the Z direction becomes zero.

III. NUMERICAL RESULTS AND DISCUSSION

For a qualitative and quantitative discussion of the dynamic behavior of the nanowire amplitudes, we consider the following system parameters: a carbon nanotube of radius $r = 1$ nm and length $L = 1 \ \mu$m [26], superconducting order parameter $\Delta_0 \sim 1$ meV, Josephson critical current $j_c \sim 100$ nA [27], and quality factor $Q \sim 10^3$ [28]. We also assume that $\tilde{\gamma} = 1/Q$, $h_z \sim 40$ mT, $\varepsilon = 0.012$, and R_T is varied from 53 to 544 nm. From Eq. (6), the control parameter will take values in the interval $0.12 \leqslant \varkappa \leqslant 1.25$.

Numerical simulations of Eqs. (5a) and (5b) allow us to study the time average of the nanotube deflection coordinates $Y(\tau)$ and $Z(\tau)$ as functions of the driving voltage $\tilde{V}$. In doing so, one can notice that the system response presents a series of resonance peaks at integer values of the driving voltage, i.e., the amplitude of the nanoresonator is not damped provided the resonant condition is fulfilled: the Josephson frequency matches the mechanical frequency (see Fig. 2). This resonant phenomenon was first studied by Sonne *et al.* [23], who attributed a direct resonance at $\tilde{V} = 1$ and a parametric resonance at $\tilde{V} = 2$. Accordingly, the same conclusion can be drawn from the results presented in Fig. 2. In the remainder of the article, we will be mainly focusing on the parametric regime and take $\tilde{V} = 2$. In this case, the dynamic behavior of the amplitudes can be analyzed by postulating a solution for both deflection coordinates in the form

$$Y(\tau) = A_r(\tau)\cos(\tau) + A_i(\tau)\sin(\tau), \qquad (7a)$$

$$Z(\tau) = B_r(\tau)\cos(\tau) + B_i(\tau)\sin(\tau). \qquad (7b)$$

Here, A_i; B_i and A_r; B_r are the in-phase and quadrature amplitude components of the proposed ansatz for Y; Z given by Eq. (7), respectively. On condition that $\tilde{\gamma}, \varepsilon, \varepsilon\varkappa \ll 1$, the four envelopes in the vector $\mathbf{X} = [A_r(\tau), A_i(\tau), B_r(\tau), B_i(\tau)]$ vary slowly in time, i.e., $d\mathbf{X}/d\tau \ll 1$ and, an averaging method [29] can be employed in order to derive the equation of motion for $\mathbf{X}$. By substituting the ansatz provided in Eqs. (7) into the system of equations in Eqs. (5) and integrating over the fast

oscillations, one gets

$$\frac{dA_r}{d\tau} + \frac{\tilde{\gamma} A_r}{2} = \frac{\partial \mathcal{G}}{\partial A_i}, \quad \frac{dB_r}{d\tau} + \frac{\tilde{\gamma} B_r}{2} = \frac{\partial \mathcal{G}}{\partial B_i},$$
$$\frac{dA_i}{d\tau} + \frac{\tilde{\gamma} A_i}{2} = -\frac{\partial \mathcal{G}}{\partial A_r}, \quad \frac{dB_i}{d\tau} + \frac{\tilde{\gamma} B_i}{2} = -\frac{\partial \mathcal{G}}{\partial B_r}, \qquad (8)$$

where

$$\mathcal{G}(\varkappa) = -\frac{\varepsilon}{2\pi} \int_{-\pi}^{\pi} \cos\{[1 + \varkappa B_r \cos(\Theta) + \varkappa B_i \sin(\Theta)]$$
$$\times [A_r \cos(\Theta) + A_i \sin(\Theta) + 2\Theta]\} d\Theta. \qquad (9)$$

Here, $\mathcal{G}(\varkappa)$ is the generating Hamiltonian function for Eqs. (8).

The study proceeds by performing a stability analysis based on Eqs. (8). In general, we shall study solutions of a system of coupled ordinary differential equations (ODEs), $d\mathbf{X}/d\tau = \mathbf{f}(\mathbf{X}, \varkappa)$, and solutions of a system of algebraic equations $\mathbf{0} = \mathbf{f}(X, \varkappa)$. The discussion commences by highlighting the symmetric nature of the stationary solutions for the algebraic system in Eqs. (8). For the above considered system parameters with $\varkappa = 0.12$ ($R_T = 544$ nm), numerical simulations for the
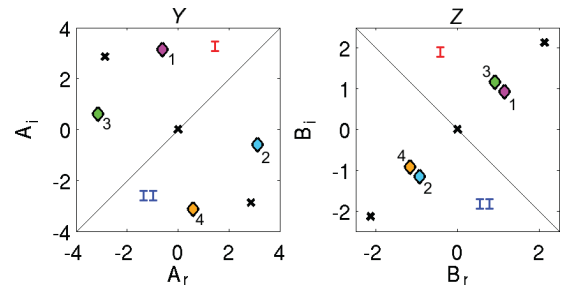
FIG. 3. (Color online) Numerical simulations for the stability analysis of Eqs. (8). Stable and unstable stationary points are indicated by colored and numbered diamonds ($\Diamond$) and black crosses ($\times$), respectively. Diamonds of identical color and number indicate the four envelopes of the stable solution $\mathbf{X}_s$, crosses in the same region (I or II) of both phase planes belong to the same unstable solution $\mathbf{X}_u$. The zero solution $\mathbf{X} \equiv \mathbf{0}$ is unstable. Here, $\tilde{\gamma} = 0.001$, $\varepsilon = 0.012$, $\varkappa = 0.12$ ($L = 1 \ \mu$m, $h_z = 40$ mT, $R_T = 544$ nm).

slowly varying envelopes show that the system presents several stationary points. Such qualitative behavior is visualized in the phase space diagrams for the nanotube amplitudes Y and Z in Fig. 3. There, solutions pictured by colored and numbered diamonds ($\Diamond$) and black crosses ($\times$) correspond to stable and unstable stationary points, respectively. Similarly, the phase portraits are divided in two regions, denoted I and II, by diagonal symmetry axes. The symmetry axes in the Y and Z coordinates satisfy the relations $A_i - A_r = 0$ and $B_i + B_r = 0$, respectively. From Fig. 3, it follows that the presented pattern of solutions has a mirror-image symmetry with respect to the line of symmetry that divides the phase diagrams into regions I and II, where diamonds of the same color and number represent the four components of a stable computed solution $\mathbf{X}_s$, and crosses in the same region (I or II) of both phase spaces account for the envelopes of an unstable solution $\mathbf{X}_u$. From a symmetric point of view, the system is characterized by two stable and two unstable (including $\mathbf{X} \equiv \mathbf{0}$) stationary points in each region. However, the dimensionless angular momentum of the nanowire, $\mathbf{L}_x = Y dZ/d\tau - Z dY/d\tau$, in both regions is equal in magnitude but opposite in sign.

TABLE I. Bifurcation pattern in the symmetric regions of solutions I and II as a function of the control parameter $\varkappa$. Solution $\mathbf{X} \equiv \mathbf{0}$ is included.

$\varkappa$ interval	Number of stable solutions	Number of unstable solutions
$\varkappa \leqslant 0.120$	2	2
$0.120 < \varkappa \leqslant 0.125$	3	3
$0.125 < \varkappa \leqslant 0.140$	1	3

Continuing our exploration, the computed results indicate that the bistable regime is only attained for $\varkappa \leqslant 0.120$. By letting the control parameter increase further, bistability is abandoned and the number of stationary solutions of Eqs. (8) is modified as well as their stability. Indeed, Table I presents the number of stable and unstable stationary solutions in the interval $0.120 \leqslant \varkappa \leqslant 0.140$ in both regions for these equations. As can be seen from the table, the system displays a phenomenon called *branching* or *bifurcation*, which is a distinctive fingerprint of nonlinear dynamical systems [30]. The exhibited branching pattern formation can be described
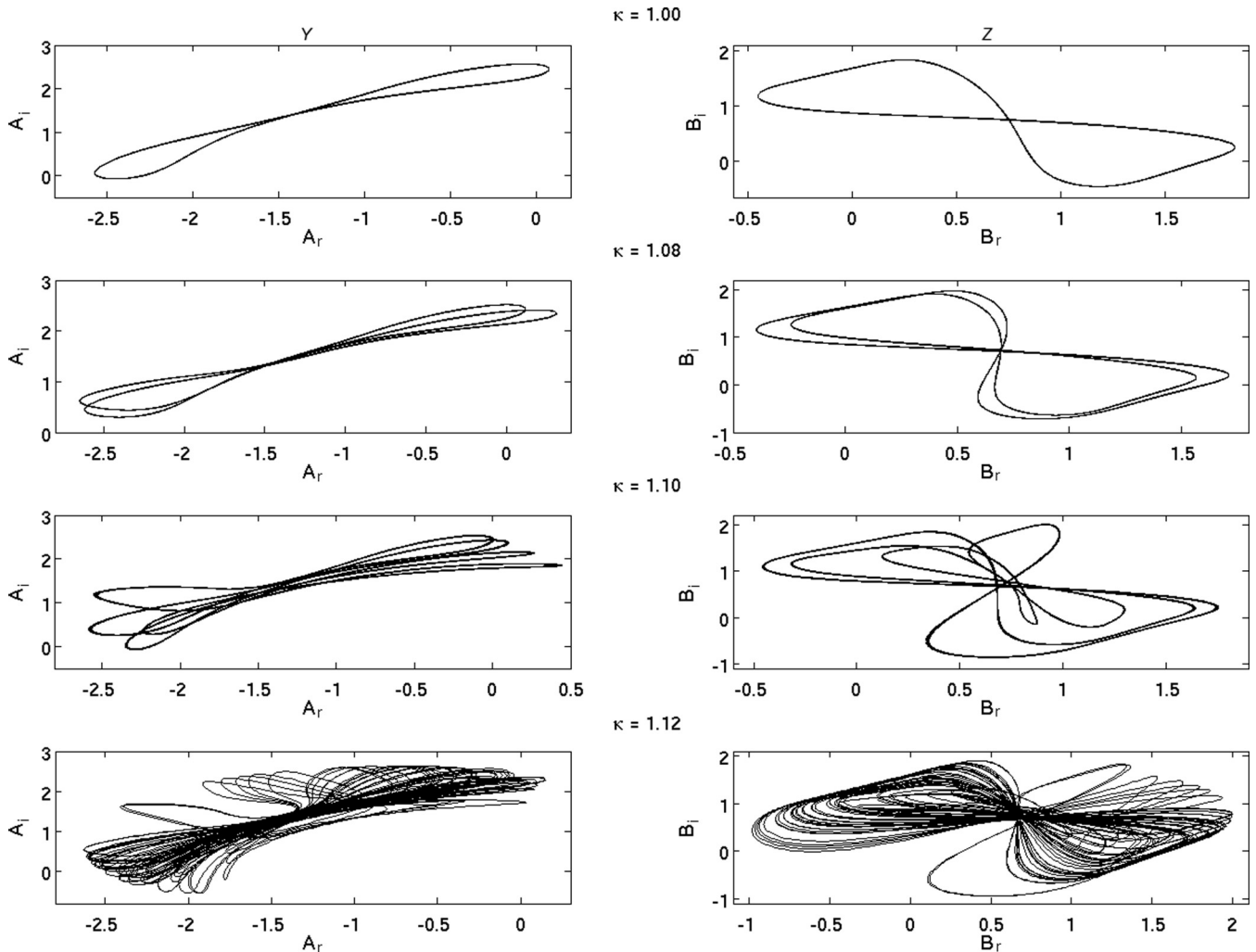
FIG. 4. Period-doubling bifurcations for different values of the control parameter. Plots are shown for the first symmetry region of both phase spaces. Simulations were obtained for $\tilde{\gamma} = 0.001$, $\varepsilon = 0.012$ ($L = 1\,\mu$m, $h_z = 40$ mT).
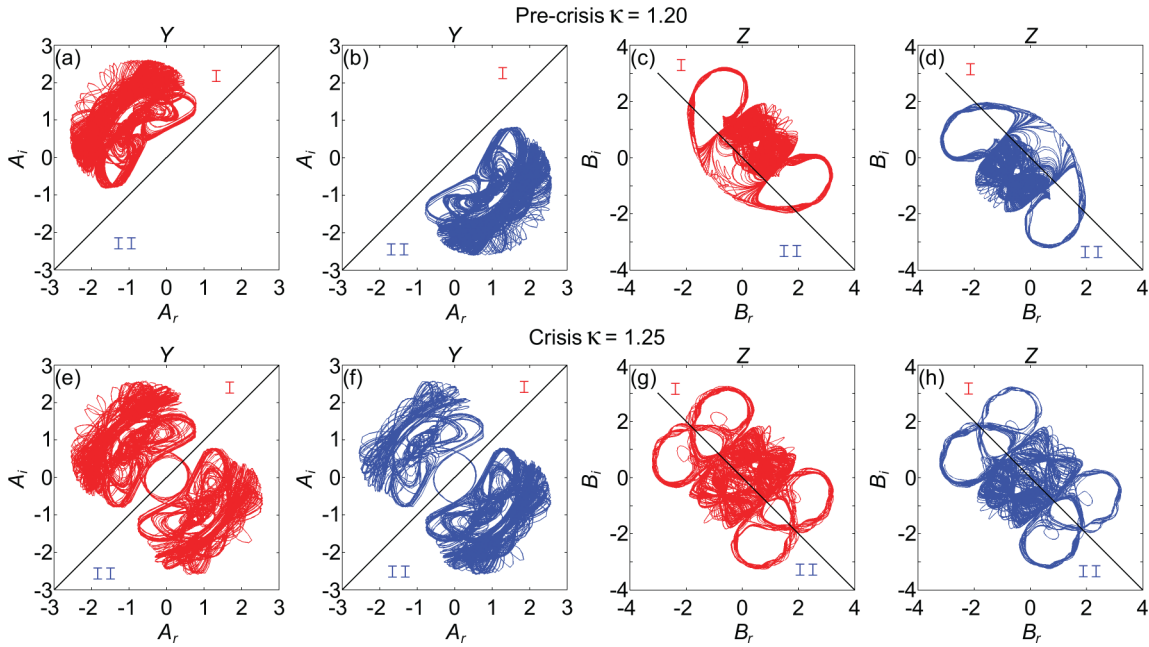
FIG. 5. (Color online) Chaotic whirling motion of the suspended carbon nanotube. In the pre-crisis regime, (a) and (b) depict the two symmetric attractors in the phase spaces for the Y component of the displacement. In (a) red lines indicate the dynamical evolution of a point with initial conditions in the first region of symmetry, region I. Its symmetric dual is shown in (b), where blue lines represent the dynamical flowing of the system for initial conditions in the second region of symmetry. For the Z component of the nanotube motion, (c) and (d) are the symmetric plots for the chaotic attractors. As before, red lines in (c) and blue lines in (d) account for the evolution of a point with initial conditions in the first and second regions of symmetry, respectively. In the crisis regime, red lines in (e) and blue lines in (f) show the single chaotic attractor formed by the two symmetric chaotic attractors joined by a periodic orbit on the basin boundary that separates them; the plot is for the dynamics in the Y component. Similarly, for the Z direction, red lines in (g) and blue lines in (h) indicate the attractor merging crisis. For the plots $\tilde{\gamma} = 0.001$, $\varepsilon = 0.01\,\mu\text{m}$, $h_z = 40$ mT).

as follows. For $\varkappa \leqslant 0.120$, bistability is accompanied by two unstable stationary points, one of them corresponds to $\mathbf{X} \equiv \mathbf{0}$ (see Fig. 3). Once the control parameter is slightly increased over the threshold value $\varkappa = 0.120$, the nonzero unstable stationary point becomes stable, and simultaneously, two new unstable solutions appear and the system has now three stable and three unstable (including the trivial solution) stationary points. Next, by varying the control parameter in the interval $0.120 \leqslant \varkappa \leqslant 0.125$, the two original stable points and the two unstable ones move in phase space and approach each other. Finally, when the control parameter ranges from 0.125 to 0.140, the bistable and the created unstable solutions coalesce into two unstable solutions. In this stage, there is only one stable and three unstable stationary points.

It turns out that for $\varkappa > 0.140$, the system leaves the regime of equilibria and enters into the one of periodic solutions. In fact, at the critical control parameter $\varkappa \sim 0.150$, there is an exchange of stability from the unique stable equilibrium to a stable limit cycle. This transformation in phase space is performed through a Poincaré-Andronov-Hopf bifurcation and the computed results show that the stable limit cycle grows in phase space for $0.150 \leqslant \varkappa \leqslant 1$. Hereupon, further changes in the control parameter will be reflected in the periodicity of the limit cycle as it can clearly be seen in Fig. 4. In this figure, the nanotube dynamics undergoes successive period-doubling cascade bifurcations in the amplitude modulation when varying $\varkappa$. Due to the symmetric character of the solutions, the results are only plotted in region I.

Period-doubling bifurcations pave the way for chaotic dynamics [31] and for the control parameter $\varkappa \sim 1.20$; the system is already within this regime. As it is shown in Figs. 5(a)–5(d), two chaotic attractors coexist and they are symmetric images of each other in the phase space. In Figs. 5(a) and 5(b), the phase portrait for the slowly varying amplitudes (A_r, A_i) for the Y component of the nanotube displacement is presented. In Fig. 5(a), red lines describe the dynamical evolution to the chaotic attractor for a point with initial conditions in the first region of symmetry of the phase space, region I. In this case, the attractor and its basin of attraction are completely located in this part of the phase portrait. Its symmetric dual is shown in Fig. 5(b), where the chaotic attractor (depicted in blue) and its basin of attraction are found to be in region number II; this plot was obtained by a simple study of the evolution of a point with initial conditions in the second region of symmetry, region II. Similarly, the qualitative description of the Z component of the nanotube displacement is also analyzed through the phase flow of the slowly varying amplitudes (B_r, B_i). This is shown in Figs. 5(c) and 5(d), where the symmetric character of the chaotic attractors is noticeable. As before, red lines indicate the dynamics of a point with initial conditions in region I and blue ones refer to the complex behavior of a point with initial conditions in the second region of symmetry II. However, there is a difference with respect to the phase portraits for (A_r, A_i). Now, the chaotic attractors are not completely located in each region of symmetry: they cross the symmetry line (that

divides the phase portrait into two parts) and enter into the other region, nevertheless, the chaotic attractors and their symmetry are very well defined.

The occurrences of sudden qualitative changes of chaotic attractors, as a parameter of the system is varied, are denoted *crises* [32,33]. In particular, an attractor merging crisis takes place for the studied system when the control parameter reaches the critical value $\varkappa_c \simeq 1.23$. In this phenomenon, the two symmetric attractors simultaneously touch a periodic trajectory or orbit on the basin boundary that separates them and merge together to form a single multipiece chaotic attractor [34,35]. The merging crisis regime can be visualized in Figs. 5(e)–5(h) where the phase portraits for the nanowire amplitudes suggest that the initially disconnected chaotic attractors, in the pre-crisis state, placed in the symmetric regions I and II are now joined. Furthermore, the flow diagrams for initial conditions in region I (red) and region II (blue) indicate that the system dynamically evolves between the two regions, i.e., the flow lines generated by Eqs. (8) and (9) are sensitive to the initial values and are dense in both regions, where the multipiece single attractor can be readily identified. In order to make the attractor merging crisis clear, we study the dynamics of the system for $\varkappa = 1.25$. The phase portraits for the Y direction have been split for two cases. Red lines in Fig. 5(e) account for the dynamics of a point with initial conditions in the first region of symmetry in the pre-crisis regime, while blue lines in Fig. 5(f) describe the dynamical evolution of a point initiated in the second region of symmetry, region II. In a similar manner, for the Z component, red lines in Fig. 5(g) represent the evolution of a point with initial conditions in region I and Fig. 5(h), the evolution of a point with initial conditions in region II.

By increasing further the control parameter, numerical studies indicate that the single attractor formed during the attractor merging crisis is suddenly destroyed (boundary crisis) and then, for parameter values above the crisis, points initialized in the region previously occupied by the former attractor appear to move in the region chaotically, but only for a finite time (chaotic transient) [32,33]. This phenomenon occurs at $\varkappa \sim 1.6$, however, this value for the control parameter corresponds to a curvature radius of about $R_T = 41$ nm, which is outside the range of curvature radius for MFM tips experimentally reported, 50–70 nm [36]. Due to this fact, the analysis of the transient chaos is not discussed in detail.

IV. CONCLUSIONS

We have considered a voltage-biased nanoelectromechanical Josephson junction, where a suspended nanowire is serving as a weak link between two superconducting electrodes, in an inhomogeneous magnetic field. For our case study, we have assumed that the magnetic field is generated by an MFM cantilever tip and the nanowire is in the form of a metallic carbon nanotube. In such a scenario, the inhomogeneity of the field in conjunction with the Josephson current flowing through the tube gives rise to a Laplace force that induces the nanoresonator to perform a whirling movement. We have studied the time evolution of the amplitude and relative phase of this nonplanar whirling motion and demonstrated that at the parametric resonance, their coupled dynamics exhibits a rich dynamical behavior characterized by multistability, limit cycles, and chaos. These stationary regimes depend on the degree of the magnetic field inhomogeneity, which in the present case, is related to the curvature radius of the magnetic cantilever tip.

The experimental implementation of the system considered in the article is plausible in light of current state-of-the-art nanofabrication techniques. For instance, Pillet and collaborators designed and constructed a superconducting hybrid nanostructure that comprises a carbon nanotube suspended between two superconductors [37]. Concerning the MFM cantilever tip, the experimental results reported by Matveev and co-workers in Ref. [36] suggest that it is possible to fabricate cantilever tips coated by a magnetic film with a curvature radius in the range of 50–70 nm with maximum magnetic fields in the range of 40–80 mT. Due to a growing interest in complex behavior in nanodevices [38], the nonlinear and nonplanar phenomena exhibited by the system studied here have potential applications in signal processing, chaotic encryption, and random number generation [24,25].

ACKNOWLEDGMENTS

[1] H. Craighead, Science **290**, 1532 (2000).

[2] M. L. Roukes, Sci. Am. **285**, 42 (2001).

[3] M. L. Roukes, Phys. World **14**, 25 (2001).

[4] A. N. Cleland, *Foundations of Nanomechanics: From Solid-State Theory to Device Applications* (Springer, Berlin, 2003).

[5] A. Cho, Science **299**, 36 (2003).

[6] K. L. Ekinci and M. Roukes, Rev. Sci. Instrum. **76**, 061101 (2005).

[7] M. Poot and H. S. van der Zant, Phys. Rep. **511**, 273 (2012).

[8] A. J. Legget, J. Phys.: Condens. Matter **14**, 415R (2002).

[9] M. P. Blencowe, Phys. Rep. **395**, 159 (2004).

[10] K. C. Schwab and M. L. Roukes, Phys. Today **58**(7), 36 (2005).

[11] I. Katz, A. Retzker, R. Straub, and R. Lifshitz, Phys. Rev. Lett. **99**, 040404 (2007).

[12] A. Cho, Science **327**, 516 (2010).

[13] M. Aspelmeyer, Nature (London) **464**, 685 (2010).

[14] R. Lifshitz and M. Cross, *Reviews of Nonlinear Dynamics and Complexity* (Wiley, Weinheim, 2009), Chap. 1, pp. 1–52.

[15] J. F. Rhoads, S. W. Shaw, and K. L. Turner, J. Dyn. Syst., Meas., Control **132**, 034001 (2010).

[16] R. B. Karabalin, M. C. Cross, and M. L. Roukes, Phys. Rev. B **79**, 165309 (2009).

[17] F. N. Mayoof and M. A. Hawwa, Chaos, Solitions Fractals **42**, 1860 (2009).

[18] M. A. Hawwa and H. M. Al-Qahtani, Comput. Mater. Sci. **48**, 140 (2010).

[19] E. Kenig, Y. A. Tsarin, and R. Lifshitz, Phys. Rev. E **84**, 016212 (2011).

[20] R. B. Karabalin, R. Lifshitz, M. C. Cross, M. H. Matheny, S. C. Masmanidis, and M. L. Roukes, Phys. Rev. Lett. **106**, 094102 (2011).

[21] Q. P. Unterreithmeier, T. Faust, and J. P. Kotthaus, Phys. Rev. B **81**, 241405 (2010).

[22] M. C. Cross, A. Zumdieck, R. Lifshitz, and J. L. Rogers, Phys. Rev. Lett. **93**, 224101 (2004).

[23] G. Sonne, R. I. Shekhter, L. Y. Gorelik, S. I. Kulinich, and M. Jonson, Phys. Rev. B **78**, 144501 (2008).

[24] W. G. Conley, A. Raman, C. M. Krousgrill, and S. Mohammadi, Nano Lett. **8**, 1590 (2008).

[25] Q. Chen, L. Huang, Y. C. Lai, C. Gragobi, and D. Dietz, Nano Lett. **10**, 406 (2010).

[26] R. Saito, G. Dresselhaus, and M. Dresselhaus, *Physical Properties of Carbon Nanotubes* (Imperial College Press, London, 1998).

[27] A. Y. Kasumov, R. Deblock, M. Kociak, B. Reulet, H. Bouchiat, I. I. Khodos, Y. B. Gorbatov, V. T. Volkov, C. Journet, and M. Bughard, Science **284**, 1508 (1999).

[28] B. Witkamp, M. Poot, and H. van der Zant, Nano Lett. **6**, 2904 (2006).

[29] A.H. Nayfeh, *Perturbation Methods* (Wiley, New York, 2000).

[30] R. Seidel, *Practical Bifurcation and Stability Analysis: From Equilibrium to Chaos* (Springer, New York, 1994).

[31] J. Argyris, G. Faust, and M. Haase, Philos. Trans. R. Soc., A **344**, 207 (1993).

[32] C. Grebogi, E. Ott, and J. A. Yorke, Phys. Rev. Lett. **48**, 1507 (1982).

[33] C. Grebogi, E. Ott, and J. A. Yorke, Phys. D (Amsterdam) **7**, 181 (1983).

[34] K. T. Chau and Zheng Wang, *Chaos in Electric Drive Systems: Analysis, Control and Application* (Wiley, Singapore, 2011).

[35] Edward Ott, *Chaos in Dynamical Systems* (Cambridge University Press, Cambridge, UK, 2002).

[36] V. N. Matveev, V. I. Levashov, V. T. Volkov, O. V. Kononenko, A. V. Chernyh, M. A. Knjazev, and V. A. Tulin, Nanotechnology **19**, 475502 (2008).

[37] J.-D. Pillet, C. H. L. Quay, P. Morfin, C. Bena, A. Levy Yeyati, and P. Joyez, Nat. Phys. **6**, 965 (2010).

[38] M. G. E. da Luz and C. Anteneodo, Philos. Trans. R. Soc., A **369**, 245 (2011).